Available online at www.sciencedirect.com

jmr&t Journal of Materials Research and Technology

journal homepage: www.elsevier.com/locate/jmrt

Original Article

Experimental investigation of selective laser melting parameters for higher surface quality and microhardness properties: taguchi and super ranking concept approaches

Rohith Sheshadri [a,**], Mohan Nagaraj [a], Avinash Lakshmikanthan [b], Manjunath Patel Gowdru Chandrashekarappa [c], Danil Yu Pimenov [d], Khaled Giasin [e], Raghupatruni Venkata Satya Prasad [f], Szymon Wojciechowski [g,*]

[a] Department of Industrial Engineering and Management, Dr. Ambedkar Institute of Technology, Visvesvaraya Technological University, Belagavi, Bangalore, 560056, India

[b] Department of Mechanical Engineering, Nitte Meenakshi Institute of Technology, Visvesvaraya Technological University, Belagavi, Bangalore, 560064, India

[c] Department of Mechanical Engineering, PES Institute of Technology and Management, Visvesvaraya Technological University, Belagavi, Shivamogga, 577204, India

[d] Department of Automated Mechanical Engineering, South Ural State University, Lenin Prosp. 76, 454080, Chelyabinsk, Russia

[e] School of Mechanical and Design Engineering, University of Portsmouth, Portsmouth, PO1 3DJ, UK

[f] Department of Materials Engineering, Indian Institute of Science, Bengaluru, 560012, Karnataka, India

[g] Faculty of Mechanical Engineering and Management, Poznan University of Technology, Poznan, 60-965, Poland

ARTICLE INFO

Article history:
Received 28 May 2021
Accepted 28 July 2021
Available online 1 August 2021

Keywords:
Selective laser melting (SLM)
Surface roughness (SR)
Inconel 625
Microhardness
Taguchi method
Super ranking concept (SRC)

ABSTRACT

In the current study, near net-shaped selective laser melting (SLM) technology was employed to build nickel-based superalloy Inconel 625 (IN625) parts with good quality. Taguchi method was employed to formulate a systematical study, analyze, and optimize the influencing factors, i.e., laser power (LP), scan speed (SS) and hatch distance (HD) on the resulting micro-hardness (MH) and surface roughness (SR) of the build samples. Scanning electron microscope (SEM) and X-ray diffraction analysis were carried out to characterize the powder morphology (spherical shaped particle possessing the size of 35 ± 6 μm) and the surface of the build samples. Laser power was the most contributing factor on the analyzed parameters (MH and SR), followed by the scanning speed and hatch distance. Taguchi determined optimal condition (MH: LP = 270 W, SS = 800 mm/s, HD = 0.08 mm; SR: LP = 270 W, SS = 800 mm/s, HD = 0.08 mm) which resulted in higher microhardness of 416 HV and lower surface roughness of 2.82 μm. Higher MH was attributed to the minimal porosity, while the uniform smooth surface of the build samples resulted in low SR as evident from the SEM images and surface texture analysis. Super ranking concept (SRC)

* Corresponding author.
** Corresponding author.
E-mail addresses: rohiths01986@gmail.com (R. Sheshadri), sjwojciechowski@o2.pl (S. Wojciechowski).

https://doi.org/10.1016/j.jmrt.2021.07.144

was used to optimize the MH and SR simultaneously, by determining a single optimal condition (LP = 300 W, SS = 600 mm/s, HD = 0.10 mm). The obtained optimal condition resulted in a MH of 382 HV, and a SR of 3.92 μm. The results of optimal conditions are validated subjected to SEM morphologies.

1. Introduction

In the 1980s, Carl Deckard and Joe Beaman were credited for the selective laser sintering (SLS) process development to manufacturing plastic prototypes [1]. Rough grainy, porous surface finish and higher shrink rates tend to alter prototypes (i.e., warp, bow, or curl) which affect the geometry of SLS parts [2]. In 1995, Fraunhofer Institute for Laser Technology, Germany, made continuous research efforts to limit the partial melting capability of SLS by introducing high power quality lasers in selective laser melting (SLM) to achieve complete melting of metal powders [2–4]. SLM process melts metal powders and deposit layer-by-layer technique to build parts with higher density which can sometime require post-processing treatment [5]. Compared to traditional manufacturing techniques (molding and tooling), SLM process possesses a wide range of technical benefits especially for manufacturing complex-shaped geometry parts such as versatility, low cost, high production rate and accuracy [6–8]. Continued research efforts proved that SLM technologies are suitable for manufacturing dental devices [9], turbo-engine [10], biomedical parts [11], bone-implants [12], hard tool steels [13] and so on.

In recent years, several investigations studied the mechanical and microstructural characterization of nickel and titanium alloy parts fabricated using SLM processes [14–16]. Parts fabricated using SLM processes offered better strength with refined grains and a more uniform distribution than those obtained from the casted or forged materials [15,16]. SLM process parameters such as scan strategy, build rate, scan speed and laser power are usually varied over a certain range to determine the optimal values which would produce the best quality parts [15,16]. SLM parameters such as laser power, energy density and scanning speed which can influence the density of the build parts, strength, microstructure, and surface roughness of maraging steel were investigated [5]. SLM factors (laser power, orientation, layer thickness and defocus distance) were investigated to study their impact on the porosity level in 17-4 PH stainless steel parts [17]. Scanning speed and hatch spacing were previously reported to be two factors that significantly influence the porosity of nickel-based superalloy fabricated using SLM [18]. The SLM variables (such as type of powder used, part geometry, machine specifications, and laser-related parameters) that influence the quality of the build parts were previously summarized in literature [19,20]. Studying, analyzing, and optimizing all factors by conducting conventional experiments can be exhaustive and impractical in industry practice due to the large number of experiments required to cover all the input parameters which might influence the final quality of the build parts. Systematic methodology represented by Design of experiments (DOE) is a powerful tool to determine the relationship between the input factors affecting a process and the analyzed outputs of that process.

Taguchi method (TM) offers reduced experimental trials with a simultaneous study of many variables to analyze and optimize the factors responsible for quality outputs. Table 1 displays the Taguchi method applied to analyze parameters (density, hardness, strength, porosity, surface roughness, shrinkage ratio and so on) by studying the influencing variables of the SLM process. Note that laser power and scan speed are the most significant parameters influenced by different outputs as reported earlier. Smaller-sized powder particles tend to result in better properties in build parts. Taguchi method is applied to optimize individual output at once, and therefore separate optimal processing conditions were found in many research investigations [5,21–23]. Therefore, the Taguchi method requires hybridization with other methods to obtain robust design of experiments, simultaneously for multiple outputs. It was also confirmed that there is still a need for research to study the effect of SLM parameters on the mechanical and surface characteristics of nickel-based superalloys. Nickel-based superalloy finds major applications in industrial gas turbines, petrochemical reactors, structural and power generator applications [24–27]. Therefore, extensive studies are required to apply multiple objective optimization methods to build parts with the desired overall quality in terms of strength, surface integrity and density.

Multi-criteria decision making (MCDM) methods were previously applied to select the suitable additive manufacturing process (SLS, material extrusion, SLM, material jetting, powder bed fusion, fused deposition modelling (FDM), direct metal deposition (DPD), 3D printing, etc.) [37,38]. MCDM methods such as analytical hierarchy process (AHP), a technique for order performance by similarity to ideal solution (TOPSIS), fuzzy AHP-TOPSIS, PROMETHEE were applied to select the best additive manufacturing process [39,40]. MCDM methods (multi-objective optimization based on ratio analysis (MOORA), grey relational analysis (GRA), TOPSIS, utility approach, desirability function approach (DFA)) proved their potential in offering better results by determining optimized machining parameters [41,42] and sand moulding processes [43,44]. Most MCDM methods require assigning weight fractions to solve conflicting criteria involved in multiple objective functions [41,45]. To determine appropriate weights for multiple objective functions, weight determination methods such as principal component analysis (PCA), criteria importance through intercriteria correlation (CRITIC), AHP, simple additive weighting (SAW) are applied [42–45]. The solutions vary with different weights assigned for the responses [42–44]. The

Table 1 – Summary of SLM variables, size and type of powders and analyzed parameters with major research findings.

Investigated parameters	Material and powder particle average size (μm)	Analyzed parameters	Main findings	Reference
LT: 20–100 μm LP: 90–200 W	Titanium alloy(Ti6Al4V)	ρ	PD and HD contributions are more on density	[28]
PD: 35–100 μm ET: 50–200 μs HD: 50–100 μm	10–90 μm		Small particle size results in ↑ ρ	
LP: 10–20 W SS: 200–700 mm/s PF: 10–30 kHz	AISI 316L steel	SR	↑ LP and PF, ↓ SS caused ↓ SR	[29]
LP: 206–298 W SS: 900–1300 mm/s HD: 75–105 μm	316 L stainless steel 10–90 μm	SR, ρ, H	LP is significant for all SR, ρ, H SS and HD are significant for ρ, H	[21]
S: 0.035–0.055 mm HD: 0.02–0.1 mm PD: 0.005–0.065 mm ET: 0.00002–0.0003 s	Titanium (T40) 36–104 μm	P	S is not significant	[8]
S: 0.035–0.055 mm HD: 0.02–0.1 mm PD: 0.005–0.065 mm ET: 0.00002–0.0003 s	Chromium alloy (CoCrMo) 6–41 μm	P	HD and ET are significant	[8]
PT: 0.02–0.35 mm LED: 0.2–0.5 J/mm HD: 0.04–0.07 mm	Titanium (Ti6Al4V)	ρ	PT is significant	[30]
S–S: X, Y, CO, X–Y LT: 20–50 μm LP: 35–50 W	20–80 μm 17-4 PH steel	P, SR	X–Y is the best for S–S Small size powders cause higher ρ	[22]
SS: 50–150 mm/s HD: 100–160 μm	15–50 μm		LT is the most significant factor for ρ and SR	
LP: 200–350 W SS: 150–300 mm/s HD: 0.075–0.12 mm	90 W–7Ni–3Fe 4.425–24.961 μm	VED	↑ VED causes ↑ density ↑ LP is desired for ↑ ρ	[31]
LP: 240–400 W SS: 600–1000 mm/s HD: 0.09–0.15 mm	Nickel superalloy 50.3 μm	TS	↓LP, ↑ SS and middle HD causes ↑ TS	[7]
LP: 120–160 W SS: 400–600 mm/min PFR: 0.66–0.9 g/min SGF: 6–8 L/min	AlSi10Mg alloy 54–158 μm	ρ	↓SS, ↑ LP, middle values of PFR and SGF caused ↑ ρ	[32]
LP: 57–100 W SS: 180–220 mm/min	Maraging steel 40 μm	UTS, SR, ρ	LP contributes more on UTS, SR, ρ	[5]
LP: 57–100 W SS: 180–220 mm/min	316 L stainless steel	MPW, ED	↑ ED causes better surface integrity ↑ LP, ↓SS caused ↑ ED and surface structure	[33]
LP: 90–150 W SS: 400–800 mm/s LT: 0.002–0.04 mm	316 L stainless steel 15–30 μm	ρ, S-R	LP and SS influence more on ρ and S-R	[23]
LR: 0–90°	Al–Si–10Mg 30–35 μm	ρ, GS, MH, RS, SR	↓GS, SR, RS, and ↑ MH, with higher LR	[34]
LP: 75–200 W SS: 400–1200 mm/s HD: 80–120 μm LT: 20–40 μm	Ni–Ti alloy 15–53 μm	ED	↓HD and SS, mid-values of LP and LT causes ↑ ED	[35]
LP: 630 W SS: 345 mm/min PFR: 5.2 g/min OLR: 30%	Inconel 718 30–65 μm	CS and mechanical properties	Mechanical properties of parts are found to vary between casting and forging processes	[36]

ρ: density; CS: crystal size; ET: Exposure time; GS: grain size; H: Hardness; HD: Hatch distance; LED: Linear energy density; LP: Laser power; LR: Layer rotation; LT: Layer thickness; MH: microhardness; OLR: overlap rate; P: Porosity; PD: Point distance; PF: Pulse frequency; PFR: Powder feed rate; PT: Powder thickness; RS: residual stress; S: Spot size; S-R: Shrinkage ratio; S–S: Scan strategy; SFR: Shielding flow rate; SR: Surface roughness; SS: Scan speed; VED: Volumetric energy density.

MCDM methods and weight methods require complex mathematical computation and are considered a tedious task for process or manufacturing engineers to determine an optimal parameter for better quality in SLM parts. Super ranking is considered a simple and quick predictive tool for practicing engineers to predict optimal parameters for multiple outputs without the requirements of applying weight methods [46].

In the present work, Inconel 625 nickel-based alloy was used to fabricate the SLM parts. Different analysis techniques such as (SEM, XRD and EDAX) were used to visualise the Inconel 625 alloy powders and surface integrity of the build parts. Taguchi method was applied to statistically study and analyse the investigated SLM parameters: laser power, hatch distance and scanning speed on the analysed metrics (MH and SR) of the SLM parts. Pareto analysis of variance analysis was used to determine the level of contribution for each of the studies SLM parameters and their optimal levels, separately for MH and SR. The SRC is applied to conduct simultaneous optimization that determines a single optimal condition for both the outputs. SEM and surface texture analysis of SLM parts corresponding to different selective laser melting conditions were examined.

2. Materials and methods

2.1. *Fabrication of test samples*

The commercially available nickel alloy IN625 metal powder was used to manufacture the SLM parts. The average size of the metal powders procured was found to be around 35 ± 6 μm. Fig. 1 (a) and (b) depict some of the SLM-built samples having dimensions 10 mm × 10 mm x 10 mm, fabricated with an EOSINT 280 SLM machine. In recent years, experiments are planned based on a chemometric approach (i.e., multi-variate design of experiments) to analyze and optimize the variables of different processes [47–51].

Fig. 2 depicts a schematic view of the SLM system. The building platform had dimensions of 250 mm × 250 mm x 300 mm equipped with a 400 W Laser. The build canister was filled with inert gas to avoid oxidation, and the oxygen content in the canister is kept low (<0.1%). A Nd:YAG fiber laser melted the Inconel powder on the powder bed. Throughout SLM, the process surrounding was an inert argon atmosphere. The specimens are prepared with different combinations of laser power, scan speed and hatch distance varied with the ranges of 240–300 W, 600–1000 mm/s and 0.08–0.12 mm, respectively. Taguchi experimental plan (i.e., L_9 orthogonal array) was used to fabricate the SLM parts. For each parametric condition, the experiments are repeated thrice to reduce errors and increase the precision in analysis and optimization.

Fig. 3 explains the steps adopted to model and optimize the process viz. Taguchi and SRC techniques. SLM processes manufacture parts to the desired quality provided the influencing parameters are controlled appropriately. Fatigue properties are influenced by the surface roughness of the fabricated samples [52]. The porosity and formation of nickel-layered surfaces are of paramount importance, as they appear largely on the outer surface than the inner layers of the material. The uneven surface layers initiate cracks, promote stress concentration and decrease available load area that could result in reduced mechanical properties and more likely the component fails catastrophically during their service life [53].

The study evaluates the effect of several SLM parameters on the microhardness and surface roughness. The input parameters and their levels are set after conducting trial experiments, expert's opinions, and past studies in the open literature [7,21,28,31]. Taguchi L_9 experimental matrix is suitable for three control variables operating at respective three levels. Each combination of build parameters used to fabricate were repeated two additional times to ensure that collected data are accurate and repeatable for further analysis and optimization. Before analysis, all the experimental output data are transformed to signal-to-noise (S/N) ratio data with higher the better for MH and lower-the-better for SR. The input variable contributions and optimal levels are estimated for each output (based on S/N ratio data) separately viz. Pareto analysis of variance. The determined optimal levels are validated by conducting confirmation experiments.

SLM parts are affected by multiple outputs, wherein Taguchi method limits to determine single parametric levels for multiple outputs. Taguchi method integrates the super ranking concept (SRC) with simple mathematical steps to simultaneously optimize the multiple outputs [54,55]. SRC starts with converting experimental microhardness and surface roughness data to corresponding S/N ratio data. The S/N

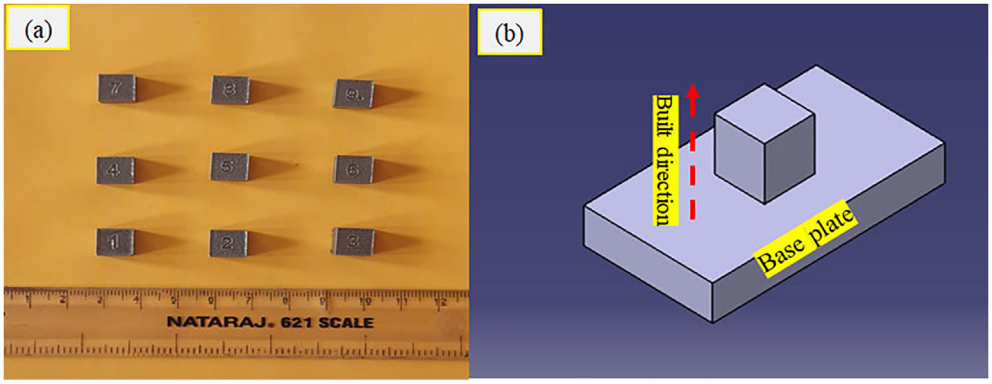

Fig. 1 – (a) SLM build samples, (b) SLM samples build direction.

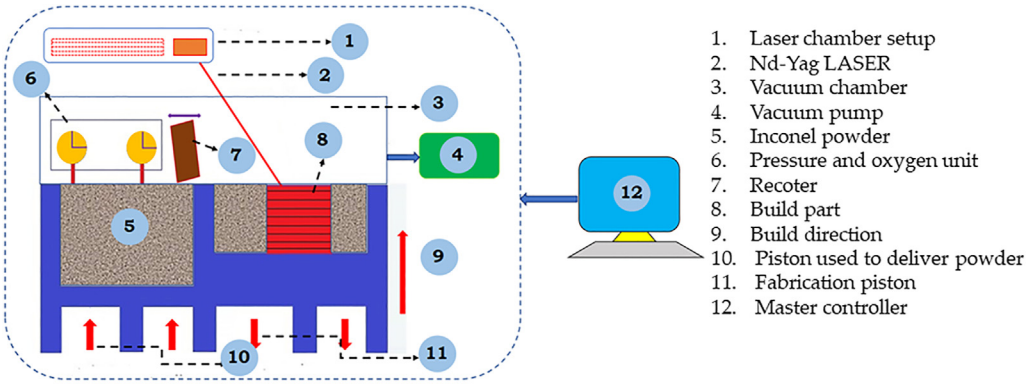

Fig. 2 – Schematic view of the SLM process.

ratio values of all nine experimental trials are ranked as per descending order. The value of the highest S/N ratio is assigned with the highest rank (i.e., rank 1) and accordingly for the rest of the experimental trials. Later, square the allotted ranks correspond to all outputs of each experimental trial and are further added to get the composite value to refer to the sum of squared rank (SSR). Factor analysis and optimal parameter levels are determined for the SSR values by conducting Pareto ANOVA. Experiments were conducted for the optimal levels and validate the model (SRC) applied for multiple-objective optimization. The framework of the proposed research work, illustrating the experimental plan and overall characterization, is presented in Fig. 4.

2.2. *Microhardness measurement*

Microhardness measurements on the SLM parts were carried out using a Vickers indenter on a microhardness machine

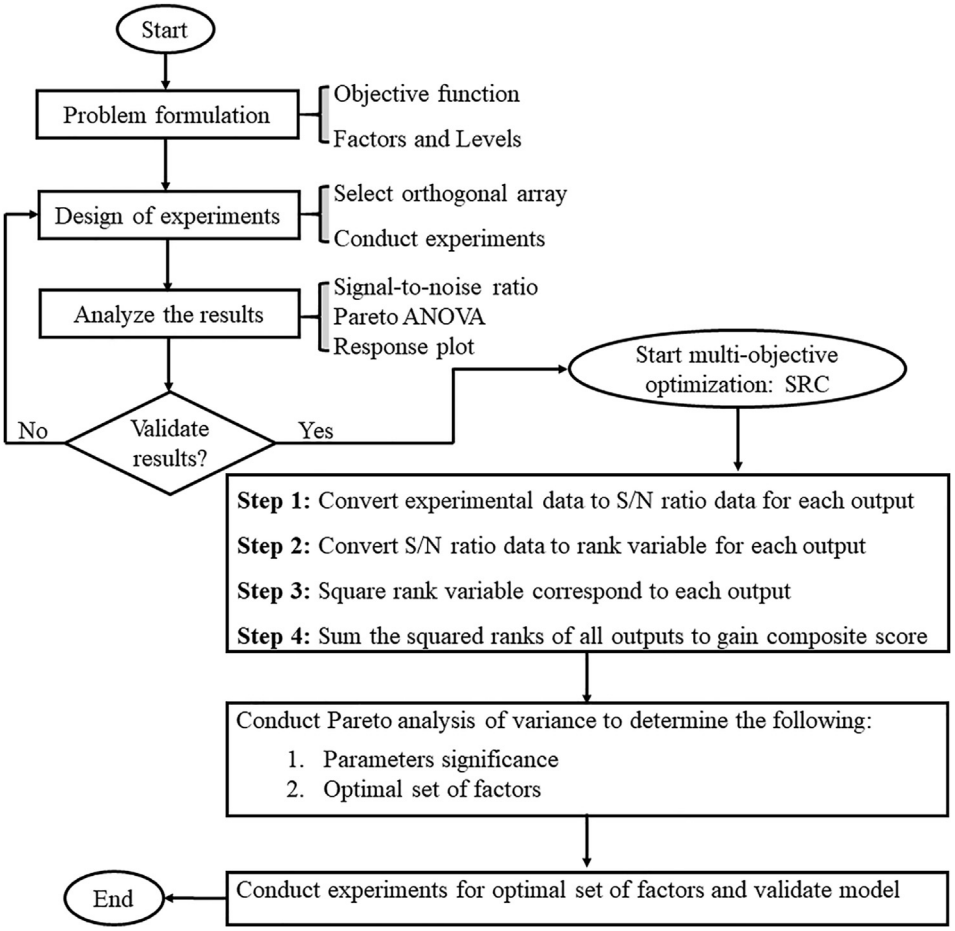

Fig. 3 – Flowchart illustrating the Taguchi and SRC employed for the SLS process.

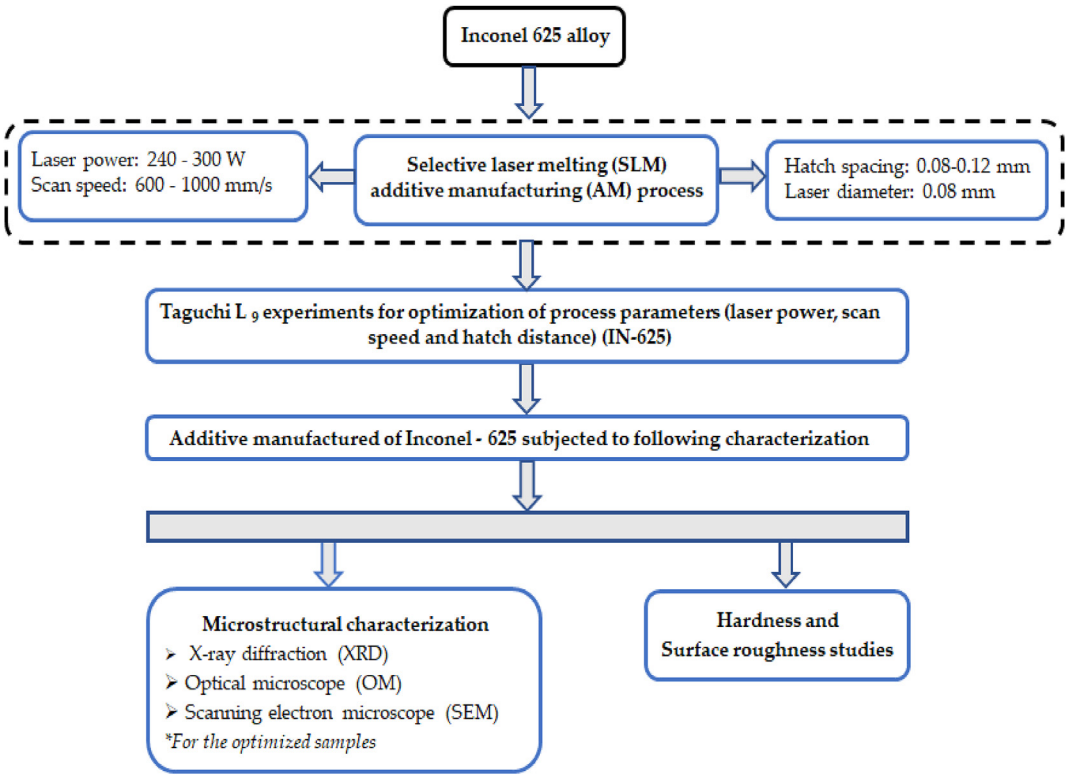

Fig. 4 – Flowchart of overall characterization used in the present work.

(Shimadzu HMV-G). The hardness values are recorded at five distinct locations on a cube (10 × 10 × 10 mm) subjected to a load of 500 g and 15 s of dwell time. For each experimental trial, an average of 15 microhardness measurements (3 replicates x 5 measurements) were used for analysis and optimization.

2.3. *Surface roughness measurement*

3D laser confocal microscope (Olympus LEXT 4000, Japan) was used to examine the surface topography of SLM parts. The use of reflected light and vertical scanning approach enables to capture of the high-resolution surface topography images in 3-dimension corresponding to SLM parts. The surface roughness measurements were carried out on each cubic face and the average of 12 roughness measurements (3 replicates x 4 measurements) were recorded for each experimental condition. The average values are used for performing the analysis and optimization of surface roughness.

2.4. *Microstructure characterisation*

The surface of the build samples was prepared as per the standard metallurgical procedures and examined under an optical (Olympus BX53M) and scanning electron microscope (Tescan Vega 3). Phase analysis characterization was carried out by applying XRD (PANanalytical X'Pert3). Fig. 4 illustrates the flowchart of the experimental plan and characterization used in the present work.

3. Results and discussion

This section discusses the results of powder characterization, microstructure, statistical analysis, and optimal levels of factors corresponding to highest microhardness and lowest surface roughness. Finally, the super ranking concept was applied to determine the single optimal set of factors and levels for multiple outputs.

3.1. *Powder characterization of Inconel 625 alloy*

EOS GmbH gas atomized Inconel 625 powder was used in the current study to print the samples viz. SLM. SEM examines the morphology of powder particles. ISO 13320 was used to analyze the distribution of powder particle size. The particles are seen to have spherical shape with an identical size distribution between 35 ± 6 μm. Fig. 5(a) presents the micrograph of gas atomized particles. A micro-dendritic structure can easily be visible under higher magnified images presented in Fig. 5(b). Fig. 5(c) shows the EDAX analysis of Inconel 625 alloy having a particle size ranging between 35 ± 6 μm. EDAX analysis confirmed the presence of nickel (57.64%) as the major element in the IN-625 powder, followed by chromium (22.06%), molybdenum (9.01%), Iron (4.02%) and traces of other elements such as C, Al, Si, Ti, V, Co, Ta and Cu. Fig. 5(d) shows the XRD analysis, which confirms the elemental composition of Ni, Cr, Mo and Fe present in IN625. Fig. 5 depicts the X-ray diffractogram of IN625, wherein the

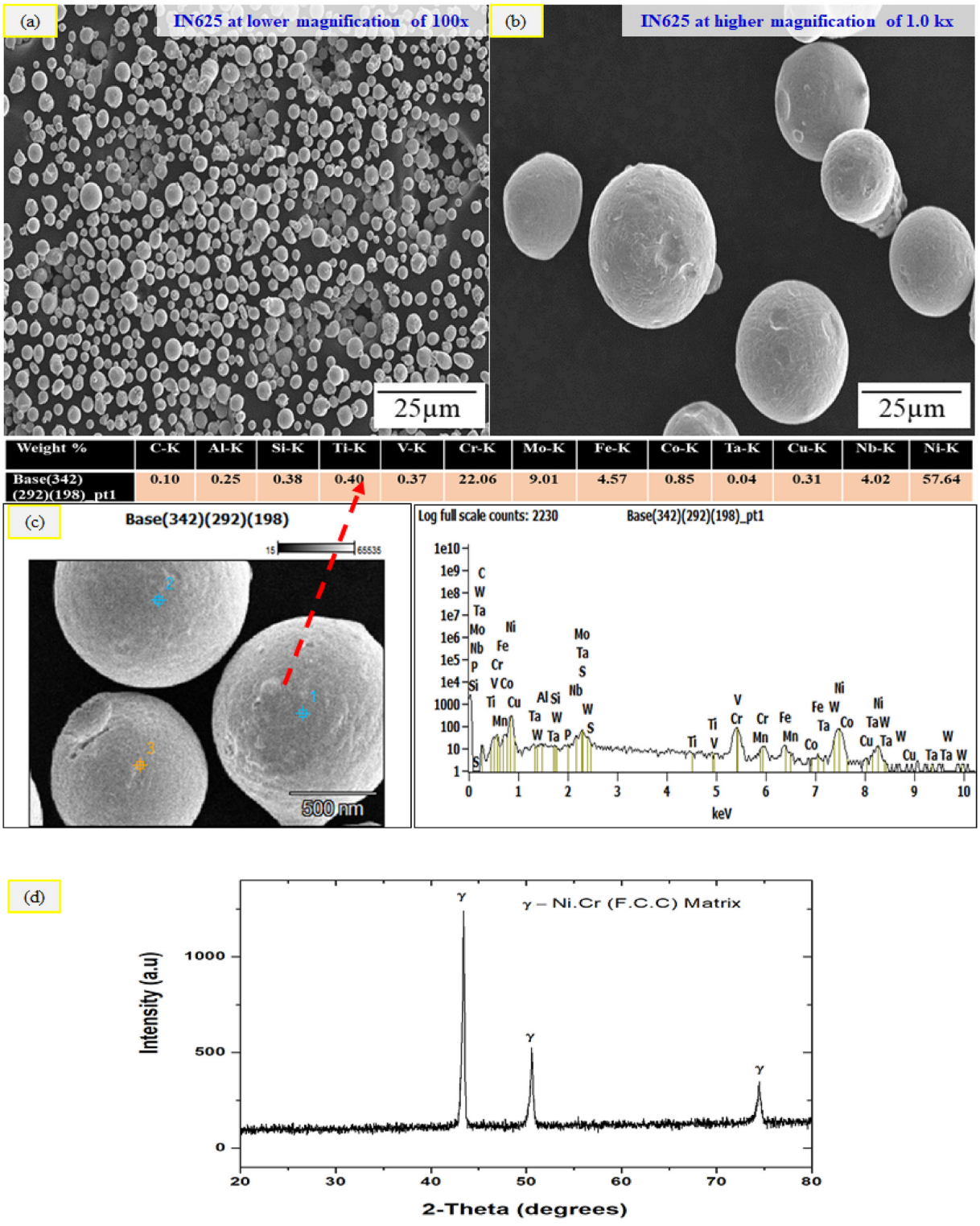

Weight %	C-K	Al-K	Si-K	Ti-K	V-K	Cr-K	Mo-K	Fe-K	Co-K	Ta-K	Cu-K	Nb-K	Ni-K
Base(342)(292)(198)_pt1	0.10	0.25	0.38	0.40	0.37	22.06	9.01	4.57	0.85	0.04	0.31	4.02	57.64

Fig. 5 – (a) and (b) Scanning electron micrographs of Inconel 625 powders at lower and higher magnification; (c) EDAX analysis of Inconel 625 powders using SEM and (d) XRD analysis of Inconel 625 alloy.

presence of γ(Ni–Cr) FCC matrix phase is shown in the IN-625 alloy.

3.2. *Experimental analysis and optimization for microhardness (MH, 0.5 HV)*

Taguchi L_9 experimental method was performed and the recorded data is given in Table 2. The output data were further analyzed for parametric analysis based on signal to noise S/N ratio and locating the optimal levels using Pareto ANOVA. Later, the optimal levels of the SLM parameters that maximize the microhardness were determined.

A higher microhardness value is always desired to obtain the best quality in SLM parts. Therefore, experimental microhardness values are transformed to S/N ratio data with higher-the-better quality characteristics. The results of the Pareto analysis of variance computed based on S/N ratio values are presented in Table 3.

The factor influence is quantified by computing the percentage contribution (refer to Table 3). Laser power resulted in the highest contribution (i.e., 68.95%), followed by scanning speed (29.03) and hatch distance (2.02%). It is important to note that the hatch distance was found to be insignificant (negligible influence) as their corresponding percent contribution was found to be lower than 5%. At low values of laser power (i.e., 240 W), there exists a comparatively lower energy density, which may not be sufficient to melt all the metal powders that resulted in irregular or discontinuous bonding, leading to lower hardness values. Contrary, higher laser power causes excess energy density, which often burns the material, resulting in low hardness values. Similar observations are reported in the literature [56]. Scanning speed at low and high values resulted in instability in the melt pool that reduces the microhardness of the SLM parts. Low scanning speed requires high temperature for melting all metal powders, and beyond the critical scanning speed results in low temperature, which may not melt all powder particles. A similar effect of the scanning speed was observed in the published literature [57]. Low values of hatch spacing resulted in an increased overlapping area of adjacent scanning lines, which in turn caused an overlying of laser beam energy. The generated uniform energy distribution between the scan lines tends to melt all powders completely and flow on already solidified scanning lines ensures strong hard-surface layers. A similar effect of negligible influence with hatch spacing was observed in recent literature [22,31]. The optimal setting of SLM parameters that maximize the microhardness of SLM parts is found equal to $LP_2SS_2HD_1$ (LP: 270 W; SS: 800 mm/s; HD: 0.08 mm). Pareto ANOVA determined the optimal levels of SLM parameters, which are found to be different from those of L_9 experiments. This occurs due to the multi-factor nature of nine experiments performed from the total of (levels $^{\text{factors}} = 3^3$) 27 experiments.

Fig. 6 show the samples of microhardness indentation (optimal and worst or normal hardness values) of IN625 produced by SLM at different process optimized parameters with different combinations of laser power (240 W and 300 W), scan speed (600 mm/s) and hatch distance (0.08 and 0.10 mm), respectively.

Table 2 – Experimental input–output of SLM process for microhardness (MH, 0.5 HV).

Exp. No.	Input variables			Measured output: MH (HV)	S/N ratio of MH (dB)
	LP, W	SS, mm/s	HD, mm		
1	240	600	0.08	356.4 ± 3.2	51.04
2	240	800	0.10	402.1 ± 2.5	52.09
3	240	1000	0.12	313.1 ± 1.4	49.91
4	270	600	0.10	319.2 ± 2.7	50.08
5	270	800	0.12	393.5 ± 1.4	51.90
6	270	1000	0.08	398.8 ± 1.1	52.02
7	300	600	0.12	337.7 ± 0.8	50.57
8	300	800	0.08	310.5 ± 2.5	49.84
9	300	1000	0.10	324.2 ± 1.6	50.22

Table 3 – Results of Pareto ANOVA for microhardness (MH, 0.5 HV).

Output		Input variables			Total
Factors		LP, W	SS, mm/s	HD, mm	
Sum at Factor Levels	1	153.04	151.69	152.90	457.67
	2	154.00	153.83	152.39	
	3	150.63	152.15	152.38	
Sum of squares of differences		18.09	7.61	0.53	26.23
Percentage contribution		68.95	29.03	2.02	100
Optimal factor levels		LP_2	SS_2	HD_1	

3.3. *Experimental analysis and optimization for surface roughness (SR, μm)*

Taguchi L_9 experiments were also performed and recorded for the surface roughness output data as shown in Table 4. Industry personnel are interested in low values of surface roughness in SLM parts. This is because, higher surface roughness of SLM parts require post-processing treatment (such as polishing, machining), which increases the manufacturing cost. Thereby, S/N ratio computation on experimental surface roughness data was carried out using "the lower-the-better" S/N ratio. The output data were further analyzed for parametric analysis and locate the optimal factor levels viz. Pareto ANOVA.

Pareto ANOVA which estimates the percentage contribution corresponding to each of the SLM parameters on the surface roughness are given in Table 5. From the analysis, the percentage highest contribution corresponds to laser power, followed by hatching distance and scanning speed with 60.61%, 33.41% and 5.98%, respectively. Low scanning speed coupled with higher laser power tends to improve the energy density, which is often sufficient to melt all powder particles that could result in lower surface roughness on SLM parts. The surface tension and viscosity correspond to melt pool decrease with lower laser power (i.e., due to insufficient energy) results in the formation of porosity in metal powders, thus causing higher SR. It was observed that lower values of hatch spacing resulted in little thermal influence corresponding to adjacent tracks which lead to lower SR. The

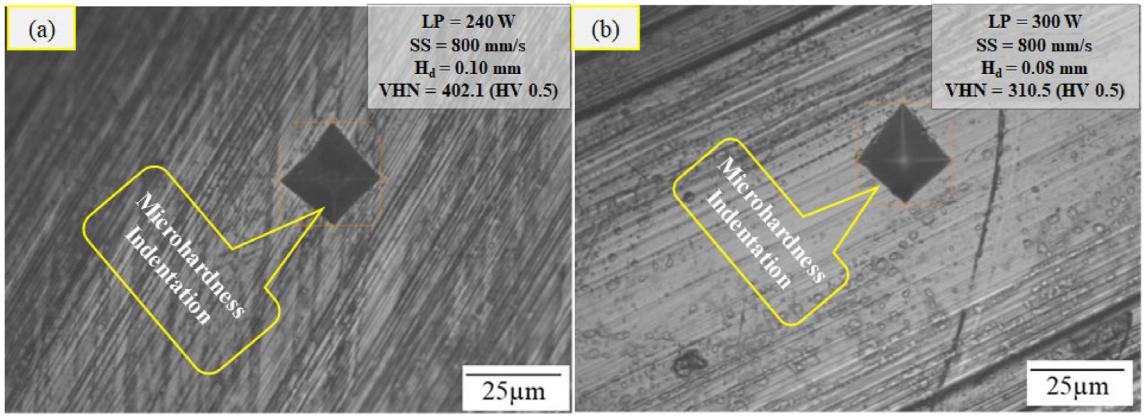

Fig. 6 – Microhardness indentation of IN625 produced by SLM at process parameter. (a): P = 240 W, SS = 800 mm/s, HD = 0.10 mm; (b): P = 300 W, SS = 800 mm/s, HD = 0.08 mm.

optimal levels ($LP_3SS_1HD_1$) corresponding to lower surface roughness may not be the exact levels of parameters used in the L_9 experiments. Similar optimal conditions with a combination of higher LP and lower scan speed were reported in the published literature [5,29].

3.4. *Multiple objective optimization: super ranking concept*

It is well-known that the multiple objective functions have many optimal solutions. These solutions are dependent based on the weights assigned to each response or output function. The super ranking concept was used to determine the single optimal set of factors and levels for multiple outputs. SRC uses simple and minimum mathematical steps that do not require assigning weight fractions for determining the optimal solutions. In SRC, the ranking of each output is done based on the S/N ratio values. A higher S/N ratio value is assigned with rank 1 and continued ranking based on descending ordered values of the S/N ratio (refer to Table 6). The sum of squared ranking (SSR) values is obtained by adding the squared ranking of MH and SR as shown in Table 6.

Pareto ANOVA was constructed based on the SSR values that could help to determine the percent contributions of factors and optimal levels. Interesting to note that the effect of the scanning speed is greater than that of the laser power (while optimizing MH and SR separately laser power showed maximum contribution, as seen in Table 5), while optimizing both outputs simultaneously. Furthermore, the hatching distance showed a significant impact with a percentage contribution of 7.62% (greater than 5%). Note that the sum of all the SSR values corresponding to each level of a factor was determined and the minimum value corresponds to the estimated three levels for a factor to determine the optimal parameter setting for the SLM process. The optimal parameter setting that simultaneously optimizes both MH and SR of the SLM process was found to be $LP_3SS_1HD_2$ as shown in Table 7. The optimal condition was also not from the L_9 experiments.

Table 4 – Experimental input–output of SLM process for surface roughness (SR, μm).

Exp. No.	Input variables			Measured output: SR (μm)	S/N ratio of SR (dB)
	LP, W	SS, mm/s	HD, mm		
1	240	600	0.08	7.88 ± 0.5	−17.93
2	240	800	0.10	9.69 ± 0.2	−19.73
3	240	1000	0.12	9.12 ± 0.4	−19.20
4	270	600	0.10	5.73 ± 0.3	−15.16
5	270	800	0.12	8.48 ± 0.1	−18.57
6	270	1000	0.08	10.91 ± 0.5	−20.76
7	300	600	0.12	6.55 ± 0.2	−16.32
8	300	800	0.08	3.80 ± 0.3	−11.60
9	300	1000	0.10	7.47 ± 0.3	−17.47

Table 5 – Results of Pareto ANOVA for surface roughness (SR, μm).

Output		Input variables			Total
Factors		LP, W	SS, mm/s	HD, mm	
Sum at Factor Levels	1	−56.86	−49.41	−50.29	−156.74
	2	−54.49	−49.9	−52.36	
	3	−45.39	−57.43	54.09	
Sum of squares of differences		219.99	121.26	21.72	362.97
Percentage contribution		60.61	33.41	5.98	100.00
Optimal factor levels		LP_3	SS_1	HD_1	

3.5. *Confirmation experiments*

Taguchi method determined optimal levels separately for both MH and SR, and are not the set of L_9 experiments. Furthermore, TM integrated SRC applied for multi-objective optimization was also determined the optimal condition different from those of L_9 experiments. Thereby, confirmation experiments were thus performed to validate the model accuracy. Note that TM determined optimal conditions for MH and SR resulted in the high values of MH and low values of SR compared to those of L_9 experiments (refer to Table 8). However, TM integrated SRC determined a single optimal

Table 6 – Multiple-objective optimization of input–output of SLM process.

Exp. No.	S/N ratio (dB)		Ranking		Squared ranking		Sum of squared ranking (SSR)
	MH, HV	SR, μm	MH, HV	SR, μm	MH, HV	SR, μm	
1	51.04	−17.93	4	5	16	25	41
2	52.09	−19.73	1	8	1	64	65
3	49.91	−19.20	8	7	64	49	113
4	50.08	−15.16	7	2	49	4	53
5	51.90	−18.57	3	6	9	36	45
6	52.02	−20.76	2	9	4	81	85
7	50.57	−16.32	5	3	25	9	34
8	49.84	−11.60	9	1	81	1	82
9	50.22	−17.47	6	4	36	16	52

Table 7 – Pareto ANOVA of multiple objective optimization results.

Output		Composite score			Total
Factors		LP, W	SS, mm/s	HD, mm	
Sum at Factor Levels	1	219	128	208	570
	2	183	192	170	
	3	168	250	192	
Sum of squares of differences		186	11,544	3042	14,772
Percentage contribution		14.39	77.99	7.62	100
Optimal factor levels		LP_3 SS_1 HD_2			

Table 8 – Summary of results of optimal conditions of SLM process.

Model and Response	Optimal condition	Responses
Taguchi method: MH	LP_2 SS_2 HD_1 (LP: 270 W; SS: 800 mm/s; HD: 0.08 mm)	MH: 416 HV SR: 5.61 μm
Taguchi method: SR	LP_3 SS_1 HD_1 (LP: 300 W; SS: 600 mm/s; HD: 0.08 mm)	MH: 355 HV SR: 2.82 μm
SRC: MH and SR	LP_3 SS_1 HD_2 (LP: 300 W; SS: 600 mm/s; HD: 0.10 mm)	MH: 382 HV SR: 3.92 μm

condition for both MH and SR, resulting in a compromising solution with moderate MH and comparatively lower surface roughness values.

3.6. *Three-dimensional surface topography of IN625 alloy at optimal and normal conditions*

The 3D surface topography at different selective laser melting conditions is presented in Fig. 7. The surface topography appears smooth uniform with limited spikes in microscale at optimal conditions: $LP_3SS_1HD_1$ (refer to Table 5), compared to normal condition $LP_3SS_3HD_1$ (refer to Table 6 of Exp. 6). Low scanning speed and hatch distance coupled with high laser power generate more energy density, which melts all the powder materials associated with little thermal influence at adjacent tracks, resulting in low surface roughness values at optimal conditions. High scan speed results in low temperature which may not be able to meet all powders result in an uneven surface at normal conditions (refer to Fig. 7(b)).

3.7. *Microstructural characterization of Inconel 625 using a scanning electron microscope at optimal and normal conditions*

Fig. 8 shows the SEM images of IN625 parts fabricated by SLM process at different parametric conditions after chromic acid etching. During laser beam scanning, traces of the melt pools

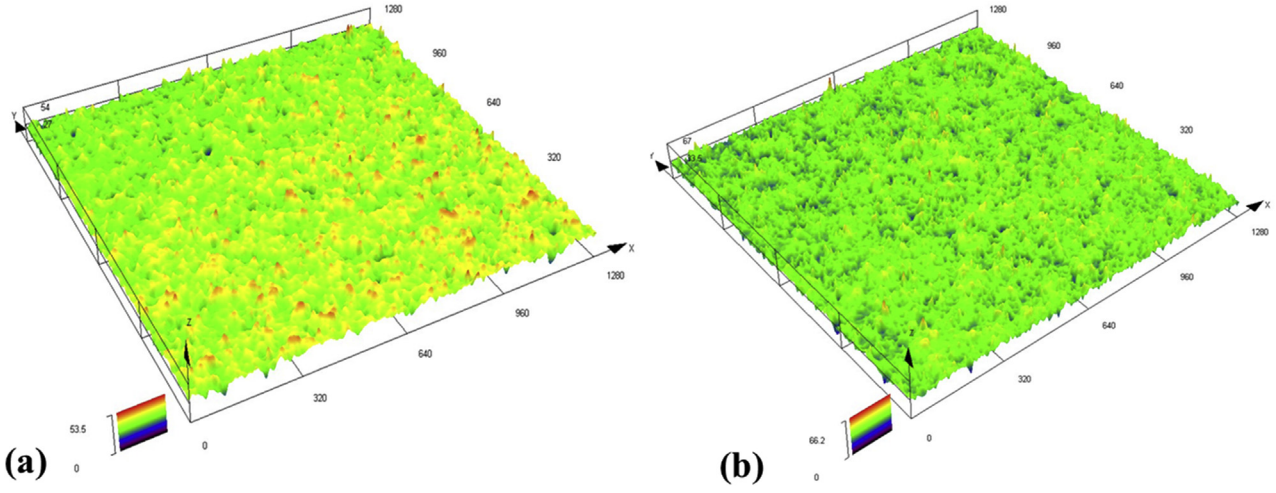

Fig. 7 – 3D surface topography of SLM parts: a) optimal condition LP_3 SS_1 HD_1 and b) normal condition LP_3 SS_3 HD_1.

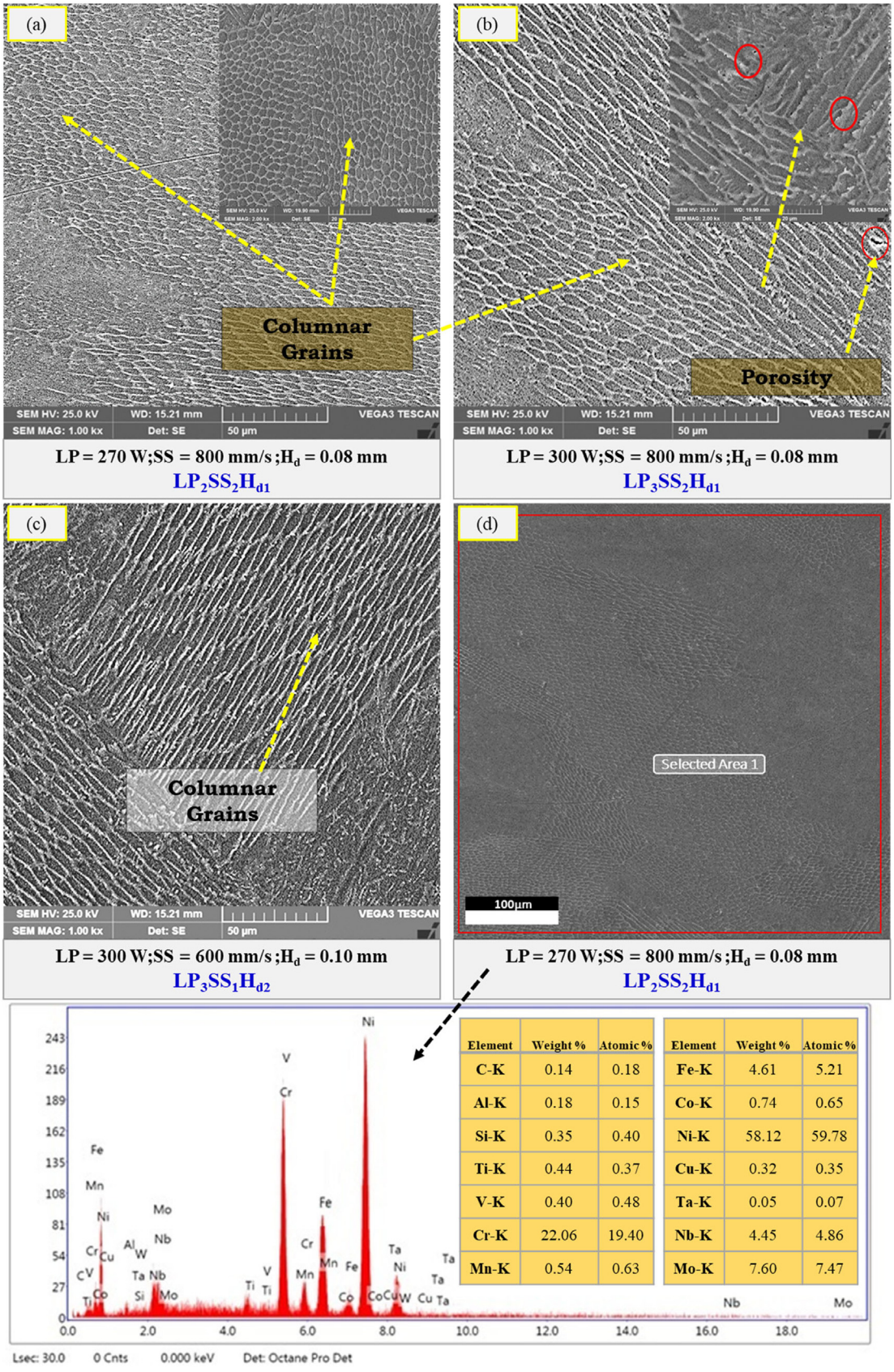

Element	Weight %	Atomic %	Element	Weight %	Atomic %
C-K	0.14	0.18	Fe-K	4.61	5.21
Al-K	0.18	0.15	Co-K	0.74	0.65
Si-K	0.35	0.40	Ni-K	58.12	59.78
Ti-K	0.44	0.37	Cu-K	0.32	0.35
V-K	0.40	0.48	Ta-K	0.05	0.07
Cr-K	22.06	19.40	Nb-K	4.45	4.86
Mn-K	0.54	0.63	Mo-K	7.60	7.47

Fig. 8 – SEM micrographs of IN625 produced by SLM. (a) Optimal condition for hardness (refer Table 3; condition: $LP_2SS_2HD_1$), (Right top image - Optimal condition for hardness at higher magnification i.e., 2000x) (b) normal process parameter conditions (refer Table 2 of Exp. 8; condition: $LP_3SS_2HD_1$), (Right top image - normal process parameter conditions at higher magnification i.e., 2000x), (c) Optimal condition for both MH and SR (refer Table 8; condition: $LP_3SS_1HD_2$), (d) EDAX analysis of IN625 (P = 270 W, SS = 800 mm/s, HD = 0.08 mm) confirming the presence of major alloying elements in IN625.

can be noticed. They seem partially overlapped owing to the assimilated laser beam approach. The laser beam could even melt an adequate amount over a frayed powder layer and hence a portion of material solidified, leading to a close bond among the strands and the initiation of columnar grains traversing several melting pools in the building direction represented in arrows, as shown in Fig. 8 (a) and (b). Fig. 8 (a) shows the SEM micrograph of IN625 alloy at optimal condition for hardness (refer to Table 3: $LP_2SS_2HD_1$). Also, from the Fig. 8 (a), right top image depicts the optimal condition for hardness at higher magnification i.e., 2000x. From Fig. 8 (a) it was observed that minimal porosity was produced at lower power of 270 W. The build sample comprised of columnar grains that raised parallel to the surface due to rapid solidification.

Fig. 8 (b) shows the SEM micrograph of IN625 at normal process parameter conditions (refer to Table 2 of Exp. 8; condition: $LP_3SS_2HD_1$). From Fig. 8 (b) we can observe an increase in porosity due to its sample produced at a high power of 300 W. Also, from the Fig. 8 (b), right top image depicts the normal process parameter condition at higher magnification i.e., 2000x. Fig. 8 (c) shows the SEM micrograph of IN625 at optimal condition for both hardness and surface roughness (refer to Table 8; condition: $LP_3SS_1HD_2$). From Fig. 8 (c), it can be observed that few porosity spots exists on the sample surface similar to that observed in Fig. 8 (b). Elements with lower melting points and impurities on the metal powder, such as oxides or moistness, can lead to porosity. These impurities can vaporize because of high power, leading to entrapment of gas, leaving the pores behind [58,59]. Further, it is also ascertained that there is a minimum average porosity and less unfused area with fine microstructure in the deposit and interface zone, leading to fast solidification with a high cooling rate, as reported by other research groups [5]. Fig. 8 (d) shows EDAX analysis of IN625 (LP = 270 W, SS = 800 mm/s, HD = 0.08 mm), confirming the presence of main alloying elements in IN625 such as Ni, Cr, Mo, Fe and Nb.

4. Conclusions

Additive manufacturing based selective laser melting (SLM) technology was successfully used to build nickel-based superalloy, i.e., Inconel 625 for different optimized process parameters. The specimens are prepared with different combinations of laser power, scan speed and hatch distance. The influence of some SLM parameters on the evolution of cast microstructure and their impact on the mechanical properties, i.e., hardness, the surface roughness of the resulting AM samples, have been investigated. Further, the Taguchi method and super ranking concepts were applied to determine optimal levels resulting in better surface quality and microhardness, validated by conducting confirmation experiments. The conclusions of the present study are outlined below.

1. IN625 samples were successfully built by AM-based selective laser melting (SLM) technology with different combinations of laser power, scan speed and hatch distance varied with the ranges of 240–300 W, 600–1000 mm/s and 0.08–0.12 mm, respectively.
2. Experimental study and multi-factor optimization towards better microhardness and surface quality of IN625 material build SLM parts are focused on the present work.
3. IN625 powder was subjected to different characterization techniques such as energy dispersive spectroscopy (EDS) and X-ray energy dispersive (XRD) spectroscopy analysis, which confirmed the presence of major constituent elements of IN625 alloy such as Ni, Cr, Mo, Nb and Fe.
4. From the microhardness and surface roughness studies of Inconel 625 deposit carried out, it was found that the optimal and normal or sub-optimal value was found out for process parameters LP = 240 W, SS = 800 mm/s, HD = 0.10 mm and LP = 300 W, SS = 800 mm/s, HD = 0.08 mm, respectively.
5. Taguchi L9 experiments with different sets of laser power, scan speed and hatch distance were studied to examine the quality (MH and SR) of SLM parts. Laser power urged as the most dominating factor, followed by scan speed and hatch distance while analyzing individually the MH and SR.
6. Taguchi method (TM) determined a separate set of optimal levels for MH and SR, and are different from those of L_9 experiments. Experiments confirmed that the determined optimal setting resulted in lower surface roughness (3.12 μm) and higher microhardness (416 HV) values compared to those obtained from the L_9 orthogonal array.
7. TM integration with SRC helps to analyze the parametric influences and locate single factor settings while optimizing simultaneously both outputs (MH and SR). The micrographs showed a refined grain structure with minimal porosity at an optimized condition.
8. Scan speed is seen to have the highest contribution, followed by laser power and hatch distance. Experimental MH and SR values of SLM parts justify the optimized condition determined viz. TM and SRC. The results can be used in industrial practice for better quality nickel-based alloy parts processed with the SLM process.
9. In this study, different parameters were considered when setting experimental conditions, obtaining the best value for each of them. However, it is known that the optimization of two or more parameters is easier, more statistically correct, and more functional if performed with a more detailed multivariate study (experimental design, chemometrics). This type of study will be done in future works, to take into account all, the relevant variables and their interactions, finding the best experimental conditions for the proper functioning of their final applications.

Scope for future work

This research work provides detailed insight of analysis and optimization of selective laser melting parameters for improving the microhardness and surface roughness on build parts. Experimental design based on response surface methodology and chemometrics for multi-variate study

could help to analyze the interactions among the input factors and identifying the best combination of selective laser melting parameter conditions for enhanced properties of the parts. Presently, the authors are working to address these issues.

Funding

This research received no external funding.

Declaration of Competing Interest

The authors declare that they have no known competing financial interests or personal relationships that could have appeared to influence the work reported in this paper.

REFERENCES

[1] Schleifenbaum H, Diatlov A, Hinke C, Bültmann J, Voswinckel H. Direct photonic production: towards high speed additive manufacturing of individualized goods. Prod Eng Res Dev 2011;5(4):359–71. https://doi.org/10.1007/s11740-011-0331-0.

[2] Mazzoli A. Selective laser sintering in biomedical engineering. Med Biol Eng Comput 2013;51(3):245–56. https://doi.org/10.1007/s11517-012-1001-x.

[3] Traini T, Mangano C, Sammons RL, Mangano F, Macchi A, Piattelli A. Direct laser metal sintering as a new approach to fabrication of an isoelastic functionally graded material for manufacture of porous titanium dental implants. Dent Mater 2008;24(11):1525–33. https://doi.org/10.1016/j.dental.2008.03.029.

[4] Tan KH, Chua CK, Leong KF, Naing MW, Cheah CM. Fabrication and characterization of three-dimensional poly (ether-ether-ketone)/-hydroxyapatite biocomposite scaffolds using laser sintering. Proc Inst Mech Eng Pt H J Eng Med 2005;219(3):183–94. https://doi.org/10.1243/2F095441105X9345.

[5] Casalino G, Campanelli SL, Contuzzi N, Ludovico AD. Experimental investigation and statistical optimisation of the selective laser melting process of a maraging steel. Opt Laser Technol 2015;65:151–8. https://doi.org/10.1016/j.optlastec.2014.07.021.

[6] Yadroitsev I, Bertrand P, Smurov I. Parametric analysis of the selective laser melting process. Appl Surf Sci 2007;253(19):8064–9. https://doi.org/10.1016/j.apsusc.2007.02.088.

[7] Wang G, Huang L, Liu Z, Qin Z, He W, Liu F, et al. Process optimization and mechanical properties of oxide dispersion strengthened nickel-based superalloy by selective laser melting. Mater Des 2020;188:108418. https://doi.org/10.1016/j.matdes.2019.108418.

[8] Joguet D, Costil S, Liao H, Danlos Y. Porosity content control of CoCrMo and titanium parts by Taguchi method applied to selective laser melting process parameter. Rapid Prototyp J 2016;22(1):20–30. https://doi.org/10.1108/RPJ-09-2013-0092.

[9] Takaichi A, Nakamoto T, Joko N, Nomura N, Tsutsumi Y, Migita S, et al. Microstructures and mechanical properties of Co–29Cr–6Mo alloy fabricated by selective laser melting process for dental applications. J Mech Behav Biomed Mater 2013;21:67–76. https://doi.org/10.1016/j.jmbbm.2013.01.021.

[10] Gasser A, Backes G, Kelbassa I, Weisheit A, Wissenbach K. Laser Additive manufacturing: laser metal deposition (LMD) and selective laser melting (SLM) in turbo-engine applications. Laser Technol J 2010;7(2):58–63. https://doi.org/10.1002/latj.201090029.

[11] Yao J, Wang Y, Wu G, Sun M, Wang M, Zhang Q. Growth characteristics and properties of micro-arc oxidation coating on SLM-produced TC4 alloy for biomedical applications. Appl Surf Sci 2019;479:727–37. https://doi.org/10.1016/j.apsusc.2019.02.142.

[12] Ataee A, Li Y, Brandt M, Wen C. Ultrahigh-strength titanium gyroid scaffolds manufactured by selective laser melting (SLM) for bone implant applications. Acta Mater 2018;158:354–68. https://doi.org/10.1016/j.actamat.2018.08.005.

[13] Wang M, Li W, Wu Y, Li S, Cai C, Wen S, et al. High-temperature properties and microstructural stability of the AISI H13 hot-work tool steel processed by selective laser melting. Metall Mater Trans B 2019;50(1):531–42. https://doi.org/10.1007/s11663-018-1442-1.

[14] Rickenbacher L, Etter T, Hövel S, Wegener K. High temperature material properties of IN738LC processed by selective laser melting (SLM) technology. Rapid Prototyp J 2013;19(4):282–90. https://doi.org/10.1108/13552541311323281.

[15] Trosch T, Strößner J, Völkl R, Glatzel U. Microstructure and mechanical properties of selective laser melted Inconel 718 compared to forging and casting. Mater Lett 2016;164:428–31. https://doi.org/10.1016/j.matlet.2015.10.136.

[16] Zhou L, Yuan T, Li R, Tang J, Wang M, Mei F. Microstructure and mechanical properties of selective laser melted biomaterial Ti-13Nb-13Zr compared to hot-forging. Mater Sci Eng, A 2018;725:329–40. https://doi.org/10.1016/j.msea.2018.04.001.

[17] Ponnusamy P, Masood SH, Ruan D, Palanisamy S, Mohamed OA. Statistical analysis of porosity of 17-4PH alloy processed by selective laser melting. IOP Conf Ser Mater Sci Eng 2017;220:12001. https://doi.org/10.1088/1757-899X/220/1/012001.

[18] Yap CY, Tan HK, Du Z, Chua CK, Dong Z. Selective laser melting of nickel powder. Rapid Prototyp J 2017;23(4):750–7. https://doi.org/10.1108/RPJ-01-2016-0006.

[19] Emmelmann C, Urbina JPC. Analysis of the influence of burst-mode laser ablation by modern quality tools. Phys Procedia 2011;12:172–81. https://doi.org/10.1016/j.phpro.2011.03.119.

[20] Amorim FL, Lohrengel A, Müller N, Schäfer G, Czelusniak T. Performance of sinking EDM electrodes made by selective laser sintering technique. Int J Adv Manuf Technol 2013;65(9–12):1423–8. https://doi.org/10.1007/s00170-012-4267-0.

[21] Jiang HZ, Li ZY, Feng T, Wu PY, Chen QS, Feng YL, et al. Factor analysis of selective laser melting process parameters with normalised quantities and Taguchi method. Opt Laser Technol 2019;119:105592. https://doi.org/10.1016/j.optlastec.2019.105592.

[22] Averyanova M, Cicala E, Bertrand P, Grevey D. Experimental design approach to optimize selective laser melting of martensitic 17-4 PH powder: part I–single laser tracks and first layer. Rapid Prototyp J 2012;18(1):28–37. https://doi.org/10.1108/13552541211193476.

[23] Liu Y, Yang Y, Wang D. Investigation into the shrinkage in Z-direction of components manufactured by selective laser melting (SLM). Int J Adv Manuf Technol 2017;90(9):2913–23. https://doi.org/10.1007/s00170-016-9596-y.

[24] Hang R, Zhao F, Yao X, Tang B, Chu PK. Self-assembled anodization of NiTi alloys for biomedical applications. Appl Surf Sci 2020:146118. https://doi.org/10.1016/j.apsusc.2020.146118.

[25] Heilmaier M, Krüger M, Saage H, Rösler J, Mukherji D, Glatzel U, et al. Metallic materials for structural applications beyond nickel-based superalloys. JOM 2009;61(7):61–7. https://doi.org/10.1007/s11837-009-0106-7.
[26] Henderson MB, Arrell D, Larsson R, Heobel M, Marchant G. Nickel based superalloy welding practices for industrial gas turbine applications. Sci Technol Weld Joi 2004;9(1):13–21. https://doi.org/10.1179/136217104225017099.
[27] Han Q, Gu Y, Wang L, Feng Q, Gu H, Johnston R, et al. Effects of TiC content on microstructure and mechanical properties of nickel-based hastelloy X nanocomposites manufactured by selective laser melting. Mater Sci Eng, A 2020;796:140008. https://doi.org/10.1016/j.msea.2020.140008.
[28] Alfaify AY, Hughes J, Ridgway K. Critical evaluation of the pulsed selective laser melting process when fabricating Ti64 parts using a range of particle size distributions. Addit Manuf 2018;19:197–204. https://doi.org/10.1016/j.addma.2017.12.003.
[29] Campanelli SL, Casalino G, Contuzzi N, Ludovico AD. Taguchi optimization of the surface finish obtained by laser ablation on selective laser molten steel parts. Procedia CIRP 2013;12:462–7. https://doi.org/10.1016/j.procir.2013.09.079.
[30] Sun J, Yang Y, Wang D. Parametric optimization of selective laser melting for forming Ti6Al4V samples by Taguchi method. Opt Laser Technol 2013;49:118–24. https://doi.org/10.1016/j.optlastec.2012.12.002.
[31] Li J, Wei Z, Zhou B, Wu Y, Chen SG, Sun Z. Densification, microstructure and properties of 90W-7Ni-3Fe fabricated by selective laser melting. Metals 2019;9(8):884. https://doi.org/10.3390/met9080884.
[32] Liu Y, Liu C, Liu W, Ma Y, Tang S, Liang C, et al. Optimization of parameters in laser powder deposition AlSi10Mg alloy using Taguchi method. Opt Laser Technol 2019;111:470–80. https://doi.org/10.1016/j.optlastec.2018.10.030.
[33] Dursun G, Ibekwe S, Li G, Mensah P, Joshi G, Jerro D. Influence of laser processing parameters on the surface characteristics of 316L stainless steel manufactured by selective laser melting. Mater Today: Proc 2020;26:387–93. https://doi.org/10.1016/j.matpr.2019.12.061.
[34] Gupta MK, Singla AK, Ji H, Song Q, Liu Z, Cai W, et al. Impact of layer rotation on micro-structure, grain size, surface integrity and mechanical behaviour of SLM Al-Si-10Mg alloy. J Mater Res Technol 2020;9(5):9506–22. https://doi.org/10.1016/j.jmrt.2020.06.090.
[35] Yu Z, Xu Z, Guo Y, Xin R, Liu R, Jiang C, et al. Study on properties of SLM-NiTi shape memory alloy under the same energy density. J Mater Res Technol 2021;13:241–50. https://doi.org/10.1016/j.jmrt.2021.04.058.
[36] Huang L, Cao Y, Li G, Wang Y. Microstructure characteristics and mechanical behaviour of a selective laser melted Inconel 718 alloy. J Mater Res Technol 2020;9(2):2440–54. https://doi.org/10.1016/j.jmrt.2019.12.075.
[37] Raigar J, Sharma VS, Srivastava S, Chand R, Singh J. A decision support system for the selection of an additive manufacturing process using a new hybrid MCDM technique. Sadhana 2020;45(1):1–14. https://doi.org/10.1007/s12046-020-01338-w.
[38] Bhowmik S. Parameters optimization of FDM for the quality of prototypes using an integrated MCDM approach. In: Additive manufacturing technologies from an optimization perspective. IGI Global; 2019. p. 199–220. https://doi.org/10.4018/978-1-5225-9167-2.ch010.
[39] Anand MB, Vinodh S. Application of fuzzy AHP–TOPSIS for ranking additive manufacturing processes for microfabrication. Rapid Prototyp J 2018;24(2):424–35. https://doi.org/10.1108/RPJ-10-2016-0160.
[40] Peko I, Gjeldum N, Bilić B. Application of AHP, fuzzy AHP and PROMETHEE method in solving additive manufacturing process selection problem. Tehnički vjesnik 2018;25(2):453–61. https://doi.org/10.17559/TV-20170124092906.
[41] Patel GCM, Kumar RS, Naidu NS. Optimization of abrasive water jet machining for green composites using multi-variant hybrid techniques. In: Optimization of manufacturing processes. Cham: Springer; 2020. p. 129–62. https://doi.org/10.1007/978-3-030-19638-7_6.
[42] Patel GCM, Kumar S, Jagadish Pimenov DY, Giasin K. Experimental analysis and optimization of EDM parameters on HcHcr steel in context with different electrodes and dielectric fluids using hybrid Taguchi-based PCA-Utility and CRITIC-Utility approaches. Metals 2021;11(3):419. https://doi.org/10.3390/met11030419.
[43] Chate GR, Patel GCM, Bhushan SB, Parappagoudar MB, Deshpande AS. Comprehensive modelling, analysis and optimization of furan resin-based moulding sand system with sawdust as an additive. J Braz Soc Mech Sci Eng 2019;41(4):1–24. https://doi.org/10.1007/s40430-019-1684-0.
[44] Chate GR, Patel GCM, Deshpande AS, Parappagoudar MB. Modeling and optimization of furan molding sand system using design of experiments and particle swarm optimization. P I Mech Eng E-J Pro 2018;232(5):579–98. https://doi.org/10.1177/2F0954408917728636.
[45] Zavadskas EK, Turskis Z. Multiple criteria decision making (MCDM) methods in economics: an overview. Technol Econ Dev Econ 2011;17(2):397–427. https://doi.org/10.3846/20294913.2011.593291.
[46] Das PP, Chakraborty S. Parametric optimization of electrochemical machining process using Taguchi method and super ranking concept while machining on Inconel 825. In: Venkata Rao R, Taler J, editors. Advanced engineering optimization through intelligent techniques. Advances in intelligent systems and computing. 949. Singapore: Springer; 2020. https://doi.org/10.1007/978-981-13-8196-6_36.
[47] Medeiros GB, de Souza PR, Retamiro KM, Nakamura CV, Muniz EC, Corradini E. Experimental design to evaluate properties of electrospun fibers of zein/poly (ethylene oxide) for biomaterial applications. J Appl Polym Sci 2021:50898. https://doi.org/10.1002/app.50898.
[48] Bella F, Imperiyka M, Ahmad A. Photochemically produced quasi-linear copolymers for stable and efficient electrolytes in dye-sensitized solar cells. J Photochem Photobiol A: Chem 2014;289:73–80. https://doi.org/10.1016/j.jphotochem.2014.05.018.
[49] Pugliese D, Bella F, Cauda V, Lamberti A, Sacco A, Tresso E, et al. A chemometric approach for the sensitization procedure of ZnO flowerlike microstructures for dye-sensitized solar cells. ACS Appl Mater Interfaces 2013;5(21):11288–95. https://doi.org/10.1021/am403527m.
[50] Miccoli B, Cauda V, Bonanno A, Sanginario A, Bejtka K, Bella F, et al. One-dimensional ZnO/gold junction for simultaneous and versatile multisensing measurements. Sci Rep 2016;6(1):1–10. https://doi.org/10.1038/srep29763.
[51] Taşpınar H, Elik A, Kaya S, Altunay N. Optimization of green and rapid analytical procedure for the extraction of patulin in fruit juice and dried fruit samples by air-assisted natural deep eutectic solvent-based solidified homogeneous liquid phase microextraction using experimental design and computational chemistry approach. Food Chem 2021;358:129817. https://doi.org/10.1016/j.foodchem.2021.129817.
[52] Linder J, Axelsson M, Nilsson H. The influence of porosity on the fatigue life for sand and permanent mould cast aluminium. Int J Fatigue 2006;28(12):1752–8. https://doi.org/10.1016/j.ijfatigue.2006.01.001.
[53] Zhao HD, Wang F, Li YY, Xia W. Experimental and numerical analysis of gas entrapment defects in plate ADC12 die

castings. J Mater Process Technol 2009;209(9):4537–42. https://doi.org/10.1016/j.jmatprotec.2008.10.028.

[54] Besseris GJ. Multi-response optimisation using Taguchi method and super ranking concept. J Manuf Technol Manag 2008;19(8):1015–29. https://doi.org/10.1108/17410380810911763.

[55] Sinha AK, Das PP. Multi-Response optimization of a light guide plate printing process using Taguchi based super ranking method. Mater Today: Proc 2020;28(2):630–5. https://doi.org/10.1016/j.matpr.2019.12.234.

[56] Wang JC, Dommati H, Hsieh SJ. Review of additive manufacturing methods for high-performance ceramic materials. Int J Adv Manuf Technol 2019;103(5):2627–47. https://doi.org/10.1007/s00170-019-03669-3.

[57] Zhang Y, Wu L, Guo X, Kane S, Deng Y, Jung YG, et al. Additive manufacturing of metallic materials: a review. J Mater Eng Perform 2018;27(1):1–13. https://doi.org/10.1007/s11665-017-2747-y.

[58] Campanelli SL, Contuzzi N, Angelastro A, Ludovico AD. Capabilities and performances of the selective laser melting process. New trends in technologies: devices, computer, communication and industrial systems. 1(1). 2010. p. 233–52. https://doi.org/10.5772/10432. Meng Joo Er, IntechOpen.

[59] Taha MA, Yousef AF, Gany KA, Sabour HA. On selective laser melting of ultra-high carbon steel: effect of scan speed and post heat treatment. Materialwiss Werkst 2012;43(11):913–23. https://doi.org/10.1002/mawe.201200030.